Journal of Fluorescence (2022) 32:1629–1638
https://doi.org/10.1007/s10895-022-02969-4

ORIGINAL ARTICLE

Structural and Electronic (Absorption and Fluorescence) Properties of a Stable Triplet Diphenylcarbene: A DFT Study

Abrar Ul Hassan[1] · Ayesha Mohyuddin[2] · Sohail Nadeem[2] · Cihat Güleryüz[3,4] · Sadaf Ul Hassan[2] · Mohsin Javed[2] · Muhammad Salman Muhsan[5]

Received: 3 February 2022 / Accepted: 5 May 2022 / Published online: 21 May 2022

Abstract

A triplet diphenylcarbene, bis[3-bromo-5-(trifluoromethyl)[1,1'-biphenyl]-4-yl]methylidene (B3B), with exceptional stability was discovered by chemists from Japan's Mie University. To investigate its different quantum chemical features, a theoretical analysis was predicated on Density Functional Theory (DFT) and Time Dependent-DFT (TD-DFT) based technique. According to the findings, the singlet–triplet energy gap (ES-T), as well as HOMO–LUMO energy bandgap ($E_{H\text{-}L}$), was found to be diminished when nucleophilicity (N) rose. We looked at the geometrical dimensions, molecular orbitals (MOs), electronic spectra, electrostatic potential, molecular surfaces, reactivity characteristics, and thermodynamics features of the title carbene (B3B). Its electronic spectra in different solvents were calculated using TD-DFT and Polarizable Continuum Model (PCM) framework. The estimated absorption maxima of B3B were seen between 327 and 340 nm, relying on the solvents, and were attributed to the $S^0 \rightarrow S^1$ transition. Estimated fluorescence spectral peaks were found around 389 and 407 nm with the S^1 and S^0 transitions being identified. Its fluorescence/absorption intensities revealed a blue shift change when the solvent polarity was increased. The least exciting state has been discovered to be the $\pi \rightarrow \pi^*$ charge-transfer (CT) phase. According to the Natural Bonding Orbital (NBO) exploration, ICT offers a significant role in chemical system destabilization. Furthermore, several hybrid features were used to determine the NLO (nonlinear optical) features (polarizability, first-order hyperpolarizability, and dipole moment). The calculated values suggest that B3B is a promising candidate for further research into nonlinear optical properties.

Keywords DFT/TD-DFT · HOMO–LUMO · $\pi \rightarrow \pi^*$ charge-transfer · Natural bonding orbital · Triplet

Introduction

There are several long-lived singlet carbenes, but finding stable identical triplet carbenes has proven more difficult to study [1]. Also, the incorporation of new functional units by C-H functionalization using carbene or metal carbene intermediaries is an essential technique for increasing molecular diversity [2]. This technique is particularly valuable because of the high reactivity of such carben(oid) precursors [3], which permits, for example, direct C-H derivatization of aromatic hydrocarbons in a tipping point way without the requirement for any (transient) guiding groups [4]. The employment of directing groups in C-H functionalization reactions involving carbene or metal carbene radicals, on the other hand, has received far less attention [5]. Although they can directly be engaged in ligand alteration at the metallic active centre, they are more energetic ligands [6]. Incorporation and reducing elimination are two basic reactions utilizing NHCs. Several research articles devoted to NHC ligands with an extra donor group have been published in the last decade [7]. Substituent NHC binders have been updated with new research articles. Nonlinear optical (NLO) based technologies have become more important in a variety of

✉ Abrar Ul Hassan
hassanabrar2016@gmail.com

1 Department of Chemistry, University of Gujrat, Gujrat 54400, Pakistan

2 Department of Chemistry, University of Management and Technology Lahore, C-II, Johar Town, Lahore, Punjab 54756, Pakistan

3 Faculty of Science and Arts, Department of Physics, Marmara University, Istanbul 34000, Turkey

4 Department of Opticianry, Altınbaş University, 34144 Istanbul, Turkey

5 Faculty of Science, Department of Chemistry, Government College University, Lahore, Pakistan

fields, such as optical computation, interactive image analysis, optical switches, dye lasers, telecommunication devices, and optical discs [8]. Modelling of diverse NLO-phores, such as physicochemical and biological electronics, instinctual nanomaterials, single-molecule dyes, and polymeric entities, is now undertaken [9].

Quantum chemical computations can reveal molecular structures, orbital dynamics, electrical characteristics, and vibrational characteristics [10]. Density Function Theory (DFT), and its extended correlational, Time Dependent-DFT (TD-DFT) based calculations are essential and widely used methods for analyzing structural shifts, reactivity, stabilization, and fluctuations in optical characteristics induced by charge transfers through dipole moment shifts [11]. It provides a close link between theoretical and experimental data and aids in the accurate prediction of molecular characteristics [12]. DFT has long been regarded as the most straightforward and cost-effective approach for predicting the Non-Linear Optical (NLO) characteristics of organic materials [13]. It also aids in the prediction of the molecular systems with their polarizability, hyperpolarizability, including dipole moments [14]. Low computing cost, adequate programming, and outstanding results with a variety of hybrid functions are all advantages of the theory [15]. As a result of the extensive theoretical research, including DFT/TD-DFT-based techniques, the DFT/TD-DFT methodologies have been applied to title carbene (B3B) in this study. which focuses on the importance of quantum chemical investigations in analyzing various aspects of this organic molecule. There hasn't been a computational investigation of **B3B** utilizing the DFT/TDDFT approach yet. The foregoing theories were used to get full structural characteristics, such as optimized structure, topologic characteristics, electrostatic potential (ESP) surface, Frontier Molecular Orbitals (FMOs), NBO analysis, and different reactivity and thermodynamic factors. The Highest Occupied and Lowest Unoccupied Molecular Orbitals (HOMO–LUMO) studies, as well as absorption and fluorescence transformations, were studied to explain the CT inside the B3B molecule. The research was carried out in a variety of solvents as well as in the gas phase. Theoretical (absorption and fluorescence wavelengths) findings were compared. Additionally, basic NLO characteristics, such as first-order polarizabilities as well as dipole moment, were calculated using different hybrid basis functions to get a better understanding of the relationship between NLO responses and molecular structure.

Methodology

The molecular structure of B3B was optimized using the Gaussian-16 program module [16] entailing the DFT approach which was reinforced with B3LYP functional [17] at 6-311G + (d,p) basis sets. Gauss-view 5.0 was used to create the molecular arrangement [18]. The introduction of these polarization functions was required to improve the display of molecule electronic structure. The stability of the molecular structure was predicted using optimization efficiencies, geometrical parameters, zero-point corrected energy, and certain thermodynamic features [19]. The DFT/TD-DFT theory based on the optimized structure can also provide other helpful information, such as interpretation of the electrostatic potential (ESP) map, FMOs, and Natural Bond Orbital (NBO) [20], NLO, and other reactive characteristics. While investigating the NLO qualities (polarizability and first-order hyper-polarizability) [21] for B3B, different separate hybrid features were investigated, along with the long-ranged functionals. Water, ethanol, acetonitrile, chloroform, tetrahydrofuran, benzene, and toluene were used to experiment with the gaseous state. The electronic transformations were also described using TD-DFT computations at B3LYP/6-311G + (d,p) [22]. An approximate analytical framework variant of the Integral Equation Formalism-PCM (IEF-PCM) was used to examine the solvent effect. For NLO properties, the following Eqs. (1) and (2) was used

$$< \alpha > 1/3(a_{xx} + a_{yy} + a_{zz}) \tag{1}$$

$$\beta_{total} = \left[\left(\beta_{xxx} + \beta_{xyy} + \beta_{xzz}\right)^2 + \left(\beta_{yyy} + \beta_{xxy} + \beta_{yzz}\right)^2 + \left(\beta_{zzz} + \beta_{xxz} + \beta_{yyz}\right)^2 \right]^{1/2} \tag{2}$$

The global parameters of reactivity (GRP) determined from HOMO/LUMO energies have also been investigated using the foundational Eqs. (3)–(9).

$$\textbf{Ionization Potential}\,(\boldsymbol{IP}) = -E_{HOMO} \tag{3}$$

$$\textbf{Electron Affinity}\,(\boldsymbol{EA}) = -E_{LUMO} \tag{4}$$

$$\textbf{Chemical Potential}\,(\boldsymbol{\mu}) = -\left(\frac{\boldsymbol{IE} + \boldsymbol{EA}}{2}\right) \tag{5}$$

$$\textbf{Hardness}\,(\boldsymbol{\eta}) = \frac{1}{2}[E_{HOMO} - E_{LUMO}] \tag{6}$$

$$\textbf{Softness}\,(\boldsymbol{\sigma}) = \frac{1}{2\eta} \tag{7}$$

$$\textbf{Electronegativity}\ (\chi) = \left(\frac{IE + EA}{2}\right) \tag{8}$$

$$\textbf{Electrophilicity}\ (\omega) = \left(\frac{\mu^2}{2\eta}\right) \tag{9}$$

The NBO analysis at DFT/B3LYP/6-311G + (d,p) was performed to better comprehend the CT connecting donor with acceptor [23]. The carbene (B3B) and its stabilising energy were estimated using second-order perturbances theory analysis in the NBO study (Eq. (10)).

$$E^{(2)} = q_i \frac{\left(F_{i,j}\right)^2}{\varepsilon_j - \varepsilon_i} \tag{10}$$

where E(2) denotes stabilization energy, qi denotes the donor's orbital occupancy i (j), and Fij denotes the off-diagonal and diagonal NBO Fock matrix components.

Results and Discussion

Thermodynamics and Geometrical Optimization

In the gaseous state, DFT/TD-DFT with 6-311G + (d,p) basis set with B3LYP functionality was utilized to optimize the ground state (GS) geometry of B3B (Fig. 1) at its energy minimum (S^0) and therefore the least excited state ES → S^1 (singlet excited states). Frequencies estimates by the computed infrared (IR) spectrum were used to confirm the optimized geometric shapes matching to the local minima without imagined frequencies [24]. The various predicted C–C and C–H bond length and orientations in between ring C-atoms, but also the different bond angles, were in the range of the expected ranges, according to the structural features. Table S1 of the supplemental material shows the geometrical characteristics (bond lengths and bond angles) of the B3B in the GS (S^0). The expected lengths of the C–C and C–H bonds are 1.42 to 1.52 Å and 1.09 to 1.11 Å, correspondingly. The bond lengths between C(5)–N(13) with C(6)–N(37) were approximately 1.46 and 1.59 Å, respectively. Except for around the CF_3 group substitutions, the calculated angles were extremely like each other when considering the different angles. The charged particle moieties on the aromatic rings might affect the ring symmetry, culminating in-ring angles just under 120° at the substitution point and marginally more than 120° at the meta and ortho locations [43]. A similar pattern can be seen for B3B, where the bond angle C(1)–C(6)–C(5) was 118.89°, while the bond angles of C(5)–C(13)–C(7) and C(31)–C(39)–C(41) were 143.1° and 120.0°, respectively. The bond angles between the exocyclic and bromo atoms C(7)–C(8)–N(33), C(1)–C(6)–N(16), and C(11)–C(12)–N(26) are 120.7° and 121.3° respectively. The presence of bulky fluoro and bromo atoms caused significant disturbances in the structure of the quinolone moiety [25], but the geometry of the benzene ring stays unchanged.

Table 1 shows the energies and thermodynamic characteristics of the described molecule calculated using frequency simulations with B3LYP/6-311G + (d,p) at 298 K in the GS. The overall dipole moment calculated by Eq. (11) [26] is greater than that of quinoline (2.02 D). This might be explained by the presence of the fluoro group.

$$\mu_{total} = \left(\mu_x^2 + \mu_y^2 + \mu_z^2\right)^{1/2} \tag{11}$$

Frontiers Molecular Orbitals

FMOs play an important role in predicting the chemistry and kinetic endurance of compounds [27], as well as their electro-optic characteristics and electronic wavelengths [28]. The HOMO and LUMO symbols represent the proclivity to accept and give electrons. The LUMO represents the molecule's electron-deficient component, whereas the HOMO

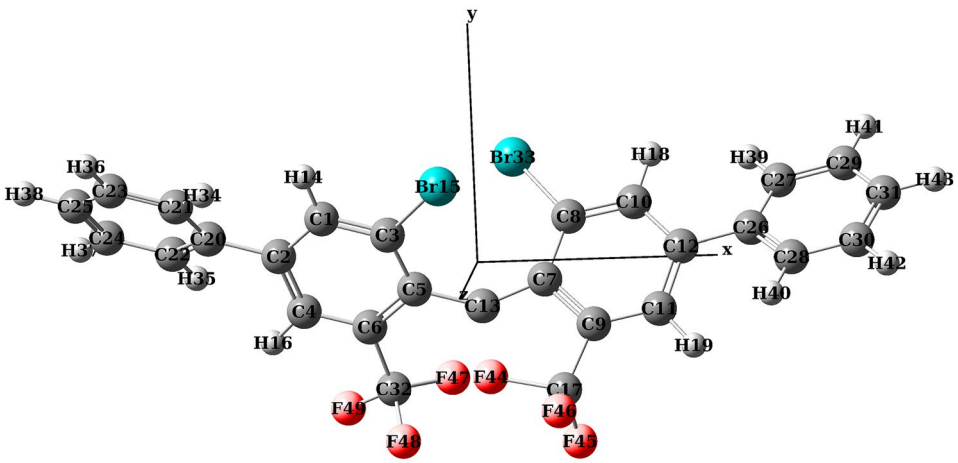

Fig. 1 Optimized molecular structure of B3B at DFT level

Table 1 Thermodynamic properties of B3B at B3LYP/6-311G + (d,p) (298 K) at GS

Parameter (298 K)	Value
SCF energy (A.U.)	–6778.980
Zero-point vibrational energy (Kcal/Mol)	220.40021
Total energy (kcal mol^{-1})	–6778.918
Rotational constants (GHZ)	
A	0.1641
B	0.0477
C	0.0425
Dipole moment	
μ_x^2	0.3813
μ_y^2	–1.2338
μ_z^2	1.1886
μ_{total}	1.7551

represents the molecule's electron-rich component. A smaller energy gap (HOMO–LUMO) can explain the molecule's putative CT interaction. The B3B molecule has 215 MOs, 151 of which were populated and 64 of which were empty. The HOMO and LUMO may be observed to be localized throughout the molecule. This indicates a significant orbital overlap between HOMO and LUMO, enabling the conversion between GS to ES [29]. The computed HOMO/LUMO energies and energy gaps are 2.70 to 2.81 eV, respectively (Fig. 2). The HOMO/LUMO interactions are taken into account when computing the reactivity coefficients using Koopmans's theorem [30]. DFT-based global reactivity specifications such as Ionization Potential (*IP*), Chemical Potential (μ), Electron Affinity (*EA*), Electronegativity (χ), Electrophilicity Index (ω), electron-donating and electron-accepting (+) power as well as hardness are important in investigating the kinetics of molecules in various environments and able to understand certain factors affiliated with the responses [31].

The *EA* and *IP* are equivalent to the molecule with its electron-accepting and donating properties and are governed by LUMO and HOMO values. The *IP* value defines the electron-donating capacity, and *IP* = 2.16 eV indicates that B3B has an admirable electron donating ability (Table 2). The positive *IP* score indicated that B3B might be used in CT responses. The energy released as an electron is injected to a neutral atom to generate an anion is referred to as Electron Affinity (EA). The computed value for the title carbene was found as -0.54 eV which showed its electron injection process to be exothermic, since nonmetals give out energy to create an anion after they absorb electrons. The value of electronegativity of a molecule is related to its ability to attract electrons and the value for present study was calculated to be 0.81. This value was much lower than that of Pauling's scale fluorine electronegativity (4 eV) to demonstrate that it had a much lower tendency to attract electrons. The title carbene (B3B) is stable, as evidenced by its negative chemical potential (-0.81). A molecule with a higher hardness value is considered more stable and reactive than molecules with its lower value. A molecule having a low value is regarded as a powerful nucleophile, whereas a molecule having a high value is called a powerful electrophile (1.35 eV). The electrophilicity

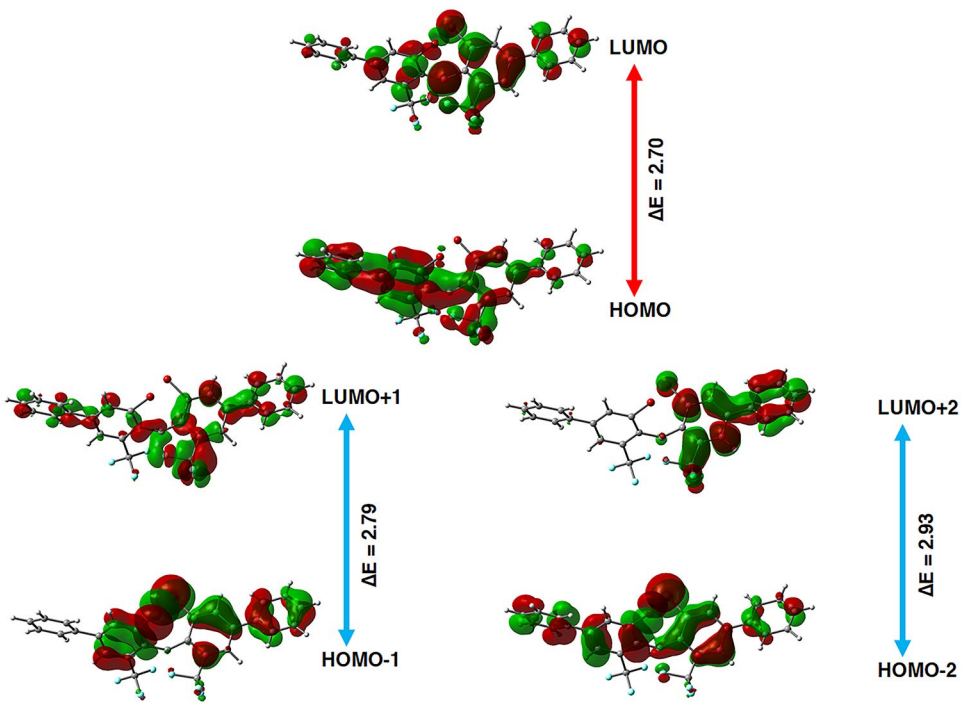

Fig. 2 Frontier Molecular Orbital analysis of B3B at DFT level

Table 2 Global Reactivity parameter values of B3B at B3LYP/6-311G + (d,p) at GS

Parameter (eV)	Value
E_H	*–2.16*
E_L	*0.54*
ΔE_{H-L}	*2.70*
(IP)	2.16
(EA)	-0.54
Electronegativity (χ)	0.81
Potential (μ)	–0.81
Hardness (η)	1.35
Softness (σ)	0.37
Electrophilicity index (ω)	0.24

index classifies compounds as powerful electrophiles having > 1.5 eV, considerable with 1.5 eV, and insignificant with 0.8 eV [32]. Current computed value of B3B (0.24 eV) showed that it might be a good electrophile.

Molecular Electrostatic Potential

The ESP mapping is extremely useful in determining the electrophilic and nucleophilic interaction areas of a compound [33]. It is depicted in diverse shades, with blue representing the positive (most electron-poor) component, green representing the neutral portion, with red representing the negative (most electron-rich) part. Figure 3 depicts the ESP map of B3B, which is between the domain of -4.25e^{-3} a.u. to + 4.25e^{-3} a.u. As one can see, B3B has a significant negative potential (red color) on the ring nitrogen atom and a weak negative potential (blue hue) on the oxygen atom. Potential (yellow hue) on the aromatic ring system, demonstrating its role as an H-bond acceptor and donor. The blue area linked with electron deficit (i.e., nucleophilic reactivity) was located surrounding the H-atoms of the Thiol group, making it a favourable location for inter-molecular H-bonding (nucleophile attack). The ESP map indicated that the charge density (red zone) was concentrated around the ring at the nitrogen atom. The pyridine ring nitrogen atom has the largest negative potential, making it a prime target for an electrophilic interaction.

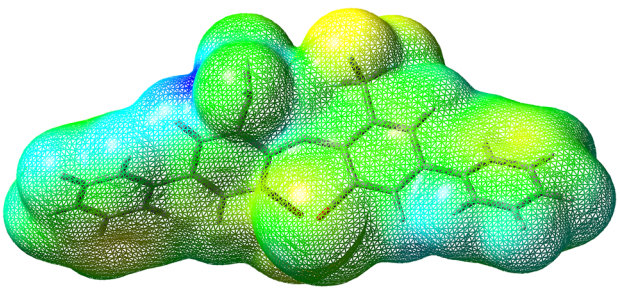

Fig. 3 MEP graph of B3B at DFT level

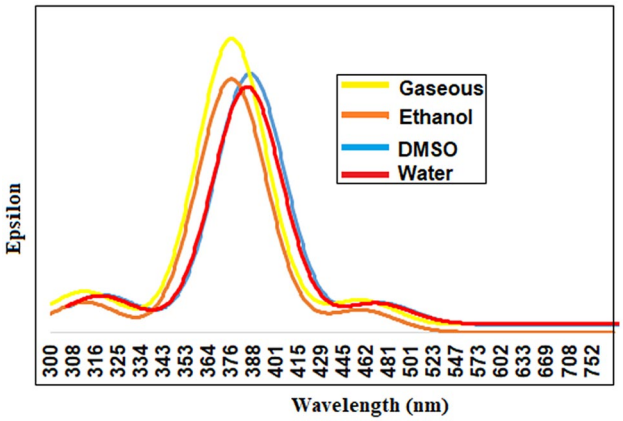

Fig. 4 TD-Electronic spectra of B3B at DFT level

Absorption and Fluorescence Studies

The absorption and fluorescence spectra of B3B (Fig. 4 and 5) were investigated using TD-DFT computations using the B3LYP functional at the 6-311G + (d,p) basis function [34]. Previously, the experimental spectra of B3B in a few solvents were documented. The solvents used in this computation include water, ethanol (EtOH) and DMSO. Table 3 summarizes the estimated vertical excitation energy with oscillator strength (OS), compositions, and assignment for B3B. The HOMO/LUMO have and composition, accordingly. It should be noted that no significant differences in the delocalization of HOMO and LUMO in different solvents were observed. The primary electronic transition band in the UV–Vis spectra of B3B is caused by HOMO → LUMO (with a 94–97%) calculated

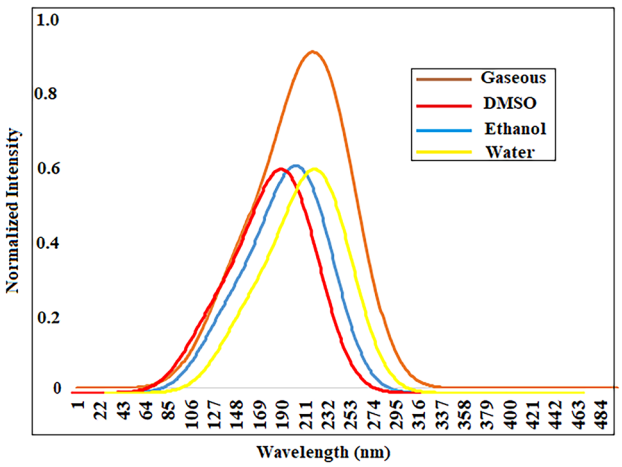

Fig. 5 TD-Fluorescence spectra of B3B at DFT level

Table 3 Computed excited-state parameters of B3B at TD-DFT/B3LYP/6-311G + (d,p) level

Solvent	State	E(cm^{-1})	Wavelength (nm)	Osc. S	Major contributions
Gaseous	1	13,742	327	0.0508	H→L (86%)
	2	19,187	421	0.4285	H→L (72%)
	3	23,970	217	0.0376	H→L + 2 (96%)
Ethanol	1	13,742	324	0.0508	H→L (86%)
	2	19,187	423	0.4285	H→L (82%)
	3	23,970	244	0.0376	H→L + 2 (76%)
DMSO	1	13,742	320	0.0508	H→L + 1 (61%)
	2	19,187	442	0.4285	H→L + 1 (80%)
	3	23,970	232	0.0376	H→L + 2 (90%)
Water	1	13,742	340	0.0508	H→L + 1 (71%)
	2	19,187	447	0.4285	H-1→L (80%)
	3	23,970	264	0.0376	H→L + 2 (56%)

between 327–340 nm dependent on the methods. The simulated UV–Vis spectra of B3B in the specified solvents and gas phase are shown in Fig. 3. The greatest absorption peak with a maximum leading to the $S^0 \rightarrow S^1$ transition was at 421, nm in the gaseous state, 423 nm in ethanol, 437 nm in ethanol and 444 nm in water. The very same (TD-DFT/B3LYP/6-311G + (d,p)) technique was used to adjust the lowest ES (S^1) of B3B in the gas phase with solvents for the fluorescence intensity. The PCM model was used to investigate the effects of solvent on the spectral properties of B3B (Table S2). The fluorescence wavelengths were acquired between 389 and 407 nm depending on the medium and were attributed to the $S^1 \rightarrow S^0$ transitions. Such fluorescence transitions have the largest oscillator intensity which occurred mostly from LUMO → HOMO transitions, as shown in spectral bands. It was discovered that when the polarity of the solvent increased, the wavelength of the fluorescence spectral maxima increased continuously. As a result, the lowest ES has associated with $\pi \rightarrow \pi^*$ transitions as a Charge Transfer (CT) state [35], which was also consistent with previous research [36]. The bathochromic shift seen experimentally agrees with the theoretical conclusions. The computed fluorescence intensity in solvents and the gas phase (Fig. 4 and Table S3) mostly contained the S^0 and S^1 state dipole moments in various solvents and gas-phase also. In the ES, the theoretically estimated dipole strength for B3B was greater than in the GS. This means that B3B was more polar in its ES state than in its GS state and that the ES state was much more stable in polar solvents than that of the GS state in aprotic and non-polar solvents [37]. The absorption/fluorescence spectra of B3B in the various solvents were recorded (Table S4) illustrating the acquired results to be agreed well with already reported results of similar structures [38]. The estimated absorption wavelengths of B3B in water were well-matched with the actual results of

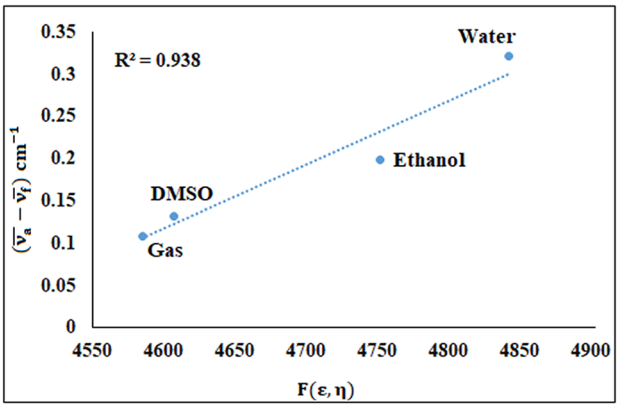

Fig. 6 Stock's shift analysis of B3B at DFT level

such relevant carbene structures and for other examined solvents, a deviation of 10–15 nm from the experimental data was noted [39]. The fluorescence wavelength in $CHCl_3$ was well-matched with the experimental data of such relevant carbene structures [40], however, there was a significant difference in the fluorescence wavelength for water and EtOH. The disparity between theoretical and experimental results might be attributable to several theoretical assumptions. The hypothesized Stokes shift in the specified solvents is closely connected to the solvent polarity function reported in SI Table S2. The research reveals a linear relationship between (ν_a)-(ν_f) and $F(\varepsilon,\eta)$ in the selected solvents (Fig. 6). In principle, the larger the $F(\varepsilon,\eta)$ the greater the Stokes shift. The Lippert-Mataga polarity indicator (Eq. (11)) was used in this work. The concentration of charges on the ring nucleophile in the S^1 state strengthens the H-bonding of both the lone pairs that enhances the redshift shift of such fluorescence s as the polarity increases. It also indicates that the H-bond to the lone pairs of the amino nitrogen atom in S^1 states, in the solvent trap, was shattered by the migration of lone pairs to the ring following excitation. As a result, the permitted transition exhibits the CT characteristic. a very small singlet–triplet gap which helps alleviate the thermally activated barrier to counteract ease of accessing; a strong singlet oscillator publicizing fluorescence in the vicinity of this small barrier; and c) increased spin–orbit coupling driving reverse intersystem crossing in this region.

Natural Bond Orbitals

The study of Natural Bond Orbitals ($NBOs_)$ offers an adequate framework for examining charge transfer and intra or intermolecular bonding in molecular systems [41]. The electron density delocalization of occupied and unoccupied NBOs is involved in the stable interaction between donor and acceptor [42]. To interpret the CT from donor

to acceptor, the NBO analysis of B3B at DFT/B3LYP/6-311G(d,p) was done. In an NBO investigation, the stabilization energy of a molecule is computed using second-order perturbation theory (see Eq. (10)). The stronger the connection between electron acceptor and donor moieties, the higher the value of E(2). The CT engagement of lone pairs of electron-donating Lone Pair (LP) atoms Br15, C17, F46, F47 and F48 with the antibonding C1-C3, C7-C9, C9-C17, C6-C32, and C6-C32 has larger stabilization energy ranging between 0.56–2.19 eV (Table 4). The high energy value is owing to a tiny energy gap between the electron source and acceptor. Also their electron acceptor transitions (π*) had very lower energies which showed their fair behavior towards accepting the electrons. Thus, the NBO examination of the title carbene demonstrated that the ICT had played a significant role in molecular system stabilization.

Nonlinear Optical Properties

We calculated the polarizability and the first hyperpolarizability of B3B at B3LYP, CAM-B3LYP, WBP7XB, and PBEPBE functional using 6-311G(d,p) to better understand the NLO behaviour [43]. The polarizability, also known as first-order hyperpolarizability, is derived by using the equations following, which use the x, y, and z components. The first-order hyperpolarizability is represented as a 3X3X3 matrix and is a rank 3 tensor. The twenty-seven components of the 3 3 3 matrices may be reduced to 10 using Kleinman symmetry. According to the frequency estimates the α_{total} and β_{total} were theoretically calculated to have 16.96 10^{24} e.s.u. and 6.28 10^{30} e.s.u values. The xxx, zzz matrices were found to be associated with more distortion of structural arrangement to generate α_{total} and β_{total} values respectively. The overall value for B3B is found to be much greater than the result for urea ($3.71X10^{31}$) e.s.u. Even though urea is a reference molecule in the measurement of NLO characteristics and is thus commonly used as a standard value for comparisons. The high hyperpolarizability valuation is usually connected to the Intramolecular Charge Transfer (ICT) qualities emitted by the movement of an electron cloud from such an electron donor area to an electron acceptor region. The NLO characteristics can be influenced by molecular geometry and the surrounding environment. Table S6 of SI contains the polarizability and first-order hyperpolarizability calculated by DFT at B3LYP/6–311(d,p) in water, EtOH, $CHCl_3$, and toluene. With increased solvent polarity, the values of dipole moment, α_{total}, and β_{total} rise. There is a large difference between these values in the gas phase and the chosen solvents. It may be deduced that

Table 4 NBO analysis of B3P at DFT level

Donor(i)	Type	Acceptor (j)	Type	E(2) [kcal/mol]	E(J)E(i) (a.u)	F(I,j) (a.u)
C1-C2	π	C2-C20	π*	1.02	1.04	0.029
C1-C3	π	C2-C4	π*	0.67	1.15	0.025
C2-C4	π	C1-C3	π*	0.83	1.13	0.027
C3-C5	π	C1-C2	π*	0.76	1.14	0.026
C6-C32	π	C2-C4	π*	2.13	1.09	0.043
C7-C8	π	C7-C9	π*	0.65	1.09	0.024
C9-C17	π	C7-C8	π*	1.50	1.12	0.037
C10-C12	π	C7-C8	π*	0.81	1.05	0.026
C11-C12	π	C7-C9	π*	0.93	1.09	0.028
C12-C26	π	C8-C10	π*	1.72	1.10	0.039
C13-F44	π	C3-C5	π*	0.67	1.02	0.024
C17-F45	π	C9-C11	π*	0.91	0.84	0.028
C20-C21	π	C2-C4	π*	0.92	1.13	0.029
C21-C23	π	C2-C20	π*	1.72	1.04	0.038
C23-C25	π	C20-C21	π*	0.85	1.14	0.028
C26-C27	π	C11-C12	π*	1.01	1.13	0.030
C27-C29	π	C12-C26	π*	1.67	1.05	0.037
C29-C31	π	C26-C27	π*	0.84	1.14	0.028
C32-F47	π	C5-C6	π*	0.59	0.72	0.021
Br15	LP	C1-C3	π*	2.19	0.75	0.036
C17	LP	C7-C9	π*	2.48	0.69	0.060
F46	LP	C9-C17	π*	7.27	0.67	0.062
F47	LP	C6-C32	π*	9.41	0.56	0.065
F48	LP	C6-C32	π*	8.79	0.56	0.063

the ICT character grows as the overall value grows. By altering the solvent polarity, the NLO responsiveness of B3B may be superficially adjusted. The total values for obtained utilizing solvatochromic techniques were 13.0 10^{30} e.s.u., 3.01X10^{25} e.s.u., and 5.21X10^{24} e.s.u., respectively. These practical quinolone derivative results can be compared to the current theoretical values. In non-polar solvents, the *βtotal* obtained for B3B coincides closely with the experimentally determined molecules to consider as good NLO entities. Although it is larger in protic and aprotic solvents, the measured *βtotal* values were smaller than B3B. As a result of the estimated values obtained using the methods described above, B3B can be considered as an attractive chemical for further NLO research.

Conclusions

The optimized B3B molecular geometry within both GS and ES, as well as its electronic spectra, structural parameters, electrostatic potential (ESP) surface, molecular orbitals (MOs), different reactivity and thermodynamics, were determined using the DFT/TD-DFT approach at the B3LYP/6-311G(d,p) level. The ESP surface of title carbene revealed that the greatest negative potential resides around the two phenyl rings, which is regarded as the preferred location of the electrophilic assault. The PCM model was used to investigate and correlate the impact of different solvents on the absorption and fluorescence spectra of B3B. The estimated absorption peaks of B3B appeared between 327—340 nm, depending on the medium, and are attributed to $S^0 \rightarrow S^1$ transitions. The fluorescence maxima were calculated between 376 and 410 nm and assigned to $S^1 \rightarrow S^0$ transitions. The lowest ES was identified as the CT state. The NBO investigation demonstrated that ICT plays a crucial role in molecular system stabilization. Furthermore, the NLO attributes (polarizability, dipole moment, and first-order hyperpolarizability) predicted by several hybrid functional indicated that B3B can be used in various NLO applications.

Contributions

AUH: Conception and design of the study. CG: acquisition of data and drafting the manuscript. AM: Resources, funding acquisition, supervision. SN: Editing the manuscript. SUH: Read the final version of the manuscript and provided valuable discussions. MJ: Revising and editing the manuscript, MSM: Formal analysis.

Supplementary Information The online version contains supplementary material available at https://doi.org/10.1007/s10895-022-02969-4.

Acknowledgements The authors are grateful to the University of Management and Technology Lahore for accessing the all-research facilities. AUH and CG are also thankful to Marmara University, Istanbul for allowing them to work on their molecular simulation lab.

Funding The authors declare that no funds, grants, or other support were received during the preparation of this manuscript.

Data Availability All data generated or analyzed during this study are included in this published article and its supplementary information file.

Code Availability Gaussian 09 W and Gauss view 5.1 are used for simulation and origin software is used to draw the plots.

Declarations

Ethics Approval Not applicable.

Consent to Participate This article does not contain any studies with human participants or animals, clinical trial registration or plant reproducibility performed by any authors.

Consent for Publication All authors have approved the paper and agree with its publication.

Research Involving Human and Animal Participants This work did not involve any human subjects.

Competing Interests The authors have no competing interests to declare that are relevant to the content of this article.

References

1. Trindle C (2003) DFT Studies of biarylcarbenes and the carbene–biradical continuum. J Org Chem 68:9669–9677. https://doi.org/10.1021/jo034753q
2. Burns NZ, Baran PS, Hoffmann RW (2009) Redox economy in organic synthesis. Angew Chem Int Ed Wiley Online Library 48:2854–2867
3. Nesterov V, Reiter D, Bag P, Frisch P, Holzner R, Porzelt A et al (2018) NHCs in main group chemistry. Chem Rev ACS Publ 118:9678–9842
4. Hossain MM, Ferdous NN, Muhib MH, Alam MS, Islam MR, Hai MA et al (2012) The effect of deactivating groups in the formation of some biologically important lactams (Isatins) and their further derivatization. J Bangladesh Chem Soc 25:46–52
5. Davies HML, Morton D (2016) Recent Advances in C–H Functionalization. J Org Chem Am Chem Soc 81:343–350. https://doi.org/10.1021/acs.joc.5b02818
6. Nohta H, Yukizawa T, Ohkura Y, Yoshimura M, Ishida J, Yamaguchi M (1997) Aromatic glycinonitriles and methylamines as pre-column fluorescence derivatization reagents for catecholamines. Anal Chim Acta Elsevier 344:233–240
7. Schuster O, Yang L, Raubenheimer HG, Albrecht M (2009) Beyond conventional N-heterocyclic carbenes: abnormal, remote,

and other classes of NHC ligands with reduced heteroatom stabilization. Chem Rev ACS Publ 109:3445–3478
8. Shanmuga Sundar GJ, Ravi Kumar SM, Sagayaraj P, Selvakumar S, Shanthi C, Sivaraj S et al (2021) Structural, mechanical, thermal, electrical, second-and third-order nonlinear optical characteristics of MCBT NLO crystal for optoelectronics device and laser applications. Bull Mater Sci Springer 44:1–8
9. Ahsin A, Ayub K (2022) Superalkali-based alkalides Li3O@[12-crown-4] M (where M= Li, Na, and K) with remarkable static and dynamic NLO properties; A DFT study. Mater Sci Semicond Process Elsevier 138:106254
10. Guo B, Xiao Q, Wang S, Zhang H (2019) 2D layered materials: synthesis, nonlinear optical properties, and device applications. Laser Photonics Rev Wiley Online Library 13:1800327
11. Üstün E, Dücsünceli SD, Özdemir I (2019) Theoretical analysis of frontier orbitals, electronic transitions, and global reactivity descriptors of M (CO) 4 L 2 type metal carbonyl complexes: a DFT/TDDFT study. Structural Chemistry, Springer 30:769–775
12. Singh G, Arora A, Rani S, Kalra P, Aulakh D, Wriedt M (2017) A family of silatrane-armed triazole-encapped salicylaldehyde-derived Schiff bases: Synthesis, spectral analysis, and antimicrobial and quantum chemical evaluation. Appl Organomet Chem 31:1–9. https://doi.org/10.1002/aoc.3728
13. Bhattacharya S, Biswas C, Raavi SSK, Krishna VS, Vamsi Krishna J, Giribabu N et al (2019) Synthesis, optical, electrochemical, DFT studies, NLO properties, and ultrafast excited state dynamics of carbazole-induced phthalocyanine derivatives. J Phys Chem C ACS Publ 123:11118–11133
14. Aydın G, Koçak O, Güleryüz C, Yavuz I (2020) Structural order and charge transfer in highly strained carbon nanobelts. New J Chem R Soc Chem 44:15769–15775. https://doi.org/10.1039/D0NJ03455J
15. Mohbiya DR, Sekar N (2018) Tuning 'Stokes Shift'and ICT Character by Varying the Donor Group in Imidazo [1, 5 a] pyridines: A Combined Optical, DFT, TD-DFT and NLO Approach. ChemistrySelect, Wiley Online Library 3:1635–1644
16. Frisch MJ, Trucks GW, Schlegel HB, Scuseria GE, Robb MA, Cheeseman JR et al (2016) G16_C01. p. Gaussian 16, Revision C.01, Gaussian, Inc., Wallin
17. Lee C, Yang W, Parr RG (1988) Development of the Colle-Salvetti correlation-energy formula into a functional of the electron density. Phys Rev B Am Phys Soc 37:785–789. https://doi.org/10.1103/PhysRevB.37.785
18. Wei LI, Xie H, Huang Y, Song L, Shao Y, Qiu K (2016) Application of Gaussian 09/GaussView 5.0 in analytical chemistry teaching. J Kunming Med Univ 37:134–136
19. Hassan AU, Sumrra SH (2021) Exploring the bioactive sites of new sulfonamide metal chelates for multi-drug resistance: An experimental versus theoretical design. J Inorg Organomet Polym Mater. https://doi.org/10.1007/s10904-021-02135-6
20. Hassan AU, Sumrra SH, Zafar MN, Nazar MF, Mughal EU, Zafar MN et al (2021) New organosulfur metallic compounds as potent drugs: synthesis, molecular modeling, spectral, antimicrobial, drug likeness and DFT analysis. Mol Diversity. https://doi.org/10.1007/s11030-020-10157-4
21. Muruganandi G, Raj MBJ (2019) Second and third-order NLO response of 2-amino-5-nitropyridinium tetrafluoroborate. Optik 182:755–760
22. Hassan AU, Sumrra SH, Imran M, Chohan ZH (2022) New 3d multifunctional metal chelates of sulfonamide: Spectral, vibrational, molecular modeling, dft, medicinal and in silico studies. J Mol Struct 132305. https://doi.org/10.1016/j.molstruc.2021.132305
23. Sumrra SH, Hassan AU, Zafar MN, Shafqat SS, Mustafa G, Zafar MN et al (2022) Metal incorporated sulfonamides as promising multidrug targets: Combined enzyme inhibitory, antimicrobial, antioxidant and theoretical exploration. J Mol Struct 1250:131710. https://doi.org/10.1016/j.molstruc.2021.131710
24. Reha D, Valdes H, Vondrasek J, Hobza P, Abu-Riziq A, Crews B et al (2005) Structure and IR spectrum of phenylalanyl-glycyl-glycine tripetide in the gas-phase: IR/UV experiments, ab initio quantum chemical calculations, and molecular dynamic simulations. Chem A Eur J1995 11:6803–6817
25. Benhamou L, Jaafar H, Thibon A, Lachkar M, Mandon D (2011) Asymmetry and steric hindrance in tripodal ligands: Reaching the limit for octahedral geometry with the newly synthesized [(6-bromo 2-pyridylmethyl)(6-fluoro 2-pyridylmethyl)(2-pyridylmethyl)] amine tripod in FeCl2 complexes. Inorganica Chim Acta 373: 195–200
26. Fantin PA, Barbieri PL, Neto AC, Jorge FE (2007) Augmented Gaussian basis sets of triple and quadruple zeta valence quality for the atoms H and from Li to Ar: Applications in HF, MP2, and DFT calculations of molecular dipole moment and dipole (hyper) polarizability. J Mol Struct THEOCHEM Elsevier 810:103–111
27. Zhang QY, Wang Y, Li SJ, Wang Y, Wei D (2022) Organocatalytic insertion into C-B bonds by in situ generated carbene: mechanism, role of the catalyst, and origin of stereoselectivity. Catal Sci Technol R Soc Chem
28. Liu C-G, Guan X-H (2013) Computational study on redox-switchable second-order nonlinear optical properties of totally inorganic Keggin-type polyoxometalate complexes. J Phys Chem C ACS Publ 117:7776–7783
29. Shah FT, Syed Z, Imam A, Raza A (2020) The impact of airline service quality on passengers' behavioral intentions using passenger satisfaction as a mediator. J Air Transp Manag 85:101815. https://doi.org/10.1016/j.jairtraman.2020.101815
30. Anguile JJ, Ngnabeuye ON, Bridget NN, Fomuta TR, Djoumbissie AL, Kuate Tagne AC et al (2018) Synthesis, characterization and DFT studies of two zinc(II) complexes based on 2-isopropylimidazole. Open J Inorg Chem 08:105–124. https://doi.org/10.4236/ojic.2018.84009
31. Kvalheim MD, Revzen S (2021) Existence and uniqueness of global Koopman eigenfunctions for stable fixed points and periodic orbits. Phys D Nonlinear Phenom Elsevier 132959
32. Sathiyaraj S, Sampath K, Butcher RJ, Pallepogu R, Jayabalakrishnan C (2013) Designing, structural elucidation, comparison of DNA binding, cleavage, radical scavenging activity and anticancer activity of copper(I) complex with 5-dimethyl-2-phenyl-4-[(pyridin-2-ylmethylene)-amino]-1,2-dihydro-pyrazol-3-one Schiff base ligand. Eur J Med Chem Elsevier Masson SAS 64:81–89. https://doi.org/10.1016/j.ejmech.2013.03.047
33. Aravindan P, Sivaraj K, Kamal C, Vennila P, Venkatesh G (2021) Synthesis, Molecular structure, Spectral Characterization, Molecular docking and biological activities of (E)-N-(2-methoxy benzylidene) anthracene-2-amine and Co(II), Cu(II) and Zn(II) complexes. J Mol Struct Elsevier B.V. 1229:129488. https://doi.org/10.1016/j.molstruc.2020.129488
34. Enamullah M, Chamayou AC, Banu KS, Kautz AC, Janiak C (2017) Copper(II)-salicylaldehydate/-methoxy(pyridine-2-yl) methanolate complexes via in-situ hydrolysis of Schiff bases. Inorg Chim Acta 464:186–194. https://doi.org/10.1016/j.ica.2017.05.001
35. Nkungli NK, Ghogomu JN, Nogheu LN, Gadre SR (2015) DFT and TD-DFT study of Bis[2-(5-Amino-[1,3,4]-Oxadiazol-2-yl) Phenol](Diaqua)M(II) Complexes [M = Cu, Ni and Zn]: Electronic structures, properties and analyses. Comput Chem 03:29–44. https://doi.org/10.4236/cc.2015.33005
36. Arbelo-López HD, Rodriguez-Mackenzie AD, Roman-Morales EM, Wymore T, López-Garriga J (2018) Charge Transfer and π to π* Transitions in the Visible Spectra of Sulfheme Met Isomeric Structures. J Phys Chem B USA 122:4947–4955. https://doi.org/10.1021/acs.jpcb.7b12393

37. Marini A, Munoz-Losa A, Biancardi A, Mennucci B (2010) What is solvatochromism? J Phys Chem B ACS Publ 114:17128–17135
38. Raut AH, Costa P, Sander W (2018) Reactions of Arylcarbenes with Lewis Acids. Chem A Eur J, John Wiley & Sons, Ltd. 24:18043–18051. https://doi.org/10.1002/chem.201803695
39. Hirai K, Bessho K, Tsujita K, Kitagawa T (2016) Diphenylcarbene protected by four ortho-iodine groups: An unusually persistent triplet carbene. Molecules. https://doi.org/10.3390/molecules21111545
40. Greisch J-F, Harding ME, Kordel M, Klopper W, Kappes MM, Schooss D (2013) Intrinsic fluorescence properties of rhodamine cations in gas-phase: triplet lifetimes and dispersed fluorescence spectra. Phys Chem Chem Phys R Soc Chem 15:8162–8170. https://doi.org/10.1039/C3CP44362K
41. Reed AE, Weinhold F (1985) Natural localized molecular orbitals. J Chem Phys 83:1736–1740. https://doi.org/10.1063/1.449360
42. Hassan AU, Guleryuz C (2021) Theoretical evaluation of the permeability of discharge item (LiOOH) in Li-O-2 batteries. Latin Am Appl Res 51:153–157. https://doi.org/10.52292/j.laar.2021.595
43. Sumathi S, Tharmaraj P, Sheela CD, Ebenezer R, Bhava PS (2011) Synthesis, characterization, NLO study, and antimicrobial activities of metal complexes derived from 3-(3-(2-hydroxyphenyl)-3-oxoprop-1-enyl)-4H-chromen-4-one and sulfanilamide. J Coord Chem, Taylor & Francis 64:1673–1682. https://doi.org/10.1080/00958972.2011.579116